

# Estimation of interplate coupling in the Nankai trough, Japan using GPS data from 1996 to 2006

Zhen Liu,<sup>1</sup> Susan Owen,<sup>1</sup> Danan Dong,<sup>1</sup> Paul Lundgren,<sup>1</sup> Frank Webb,<sup>1</sup> Eric Hetland<sup>3</sup> and Mark Simons<sup>2</sup>

<sup>1</sup>Jet Propulsion Laboratory, California Institute of Technology, Pasadena, CA 91109, USA. E-mail: zliu@jpl.nasa.gov

<sup>2</sup>Division of Geological and Planetary Sciences, California Institute of Technology, Pasadena, CA 91125, USA

<sup>3</sup>Department of Geological Sciences, University of Michigan, Ann Arbor, MI 48109, USA

Accepted 2010 March 14. Received 2010 February 2; in original form 2009 July 7

## SUMMARY

We used three-component surface velocities in southwest Japan to estimate plate coupling on the subducting plate interface at the Nankai trough. We analyzed continuous GPS data from the Japanese GEONET network from 1996 to 2006 using a consistent analysis strategy that generates bias-fixed solutions for the entire network. We applied systematic time-series analysis methods to estimate common mode error, which improved position solutions for the entire network. To allow for differences in regional deformation sources, we modelled the plate coupling on the plate interface beneath Shikoku island to Kii Peninsula and the Tokai-Suruga trough separately. The results show strong coupling at a depth of  $\sim 10$ – $30$  km off Shikoku and Kii Peninsula. The spatial variation in plate coupling coincides well with the coseismic rupture zones of the past large earthquakes. Maximum slip deficit rates of  $\sim 2$ – $3$  cm yr<sup>-1</sup> at the depth of  $\sim 5$ – $25$  km are found beneath the Tokai area, consistent with results from other studies. The downdip limits of the highly coupled areas and transition zones beneath Shikoku and the Kii Peninsula correspond approximately to estimates of the 450 °C isotherms. Good correlation is observed between the lateral variations of the slip deficit distribution, low frequency earthquakes, and coseismic slip. This correlation suggests that temperature, and possibly fluid variations, contribute to such correlation in space. The interplate slip deficit derived from the GPS velocities over the 10 yr of observations is generally compatible with the results over shorter time spans, suggesting that plate coupling in SW Japan does not change significantly over the period of these GPS measurements.

**Key words:** Satellite geodesy; Seismicity and tectonics; Subduction zone processes.

## 1 INTRODUCTION

Interseismic crustal deformation in southwest Japan is dominated by the subduction of the Philippine Sea Plate and its interaction with the overlying southwest Japan arc (Fig. 1). Over the past 1000 yr, large earthquakes ( $M = \sim 8$ ) have occurred every 100–200 yr along the Nankai trough, where the Philippine Sea Plate is subducting beneath the Amurian plate at an annual rate of  $\sim 60$ – $70$  mm yr<sup>-1</sup> (Ando 1975; Hori *et al.* 2004). Recent large earthquakes in this region include the 1944  $M7.9$  Tonankai and 1946  $M8.0$  Nankai earthquakes (Sagiya & Thatcher 1999). Since 1994, the Geographical Survey Institute (GSI) of Japan has operated the nationwide GPS Earth Observation Network (GEONET) system with more than 1200 stations (Fig. 1). Generally, the high quality data from this spatially dense network provide a unique opportunity for studying subduction zone seismic cycle deformation.

Because interseismic plate coupling contributes directly to the estimates of the occurrence and magnitude of future large earth-

quakes, many studies have used GPS data to estimate the coupling (or slip deficit) at the Philippine Sea Plate boundary in southwest Japan (e.g. El-Fiky *et al.* 1999; Ito *et al.* 1999; Ozawa *et al.* 1999; Mazzotti *et al.* 2000; Henry *et al.* 2001; Miyazaki & Heki 2001; Aoki & Scholz 2003; Jin *et al.* 2007). However, most such studies consider only horizontal GPS data, largely because of the low accuracy in the vertical component of GPS solutions. Aoki & Scholz (2003) used 2-D dislocation models and only the vertical velocities to estimate the coupling in Japan. With recent advances in data analysis and longer observations, it is now possible to use the 3-D velocity field to better constrain the slip deficit distribution on the plate interface (Sagiya 1999; Ohta *et al.* 2004; Suwa *et al.* 2006; Tabei *et al.* 2007).

In this study, we reprocessed GPS data from 1996 to 2006 for the entire GEONET (>1200 station) network in a uniform and consistent way. We developed consistent data analysis techniques to account for secular tectonic strain accumulation, coseismic offsets, post-seismic and aseismic transients, and estimated and removed

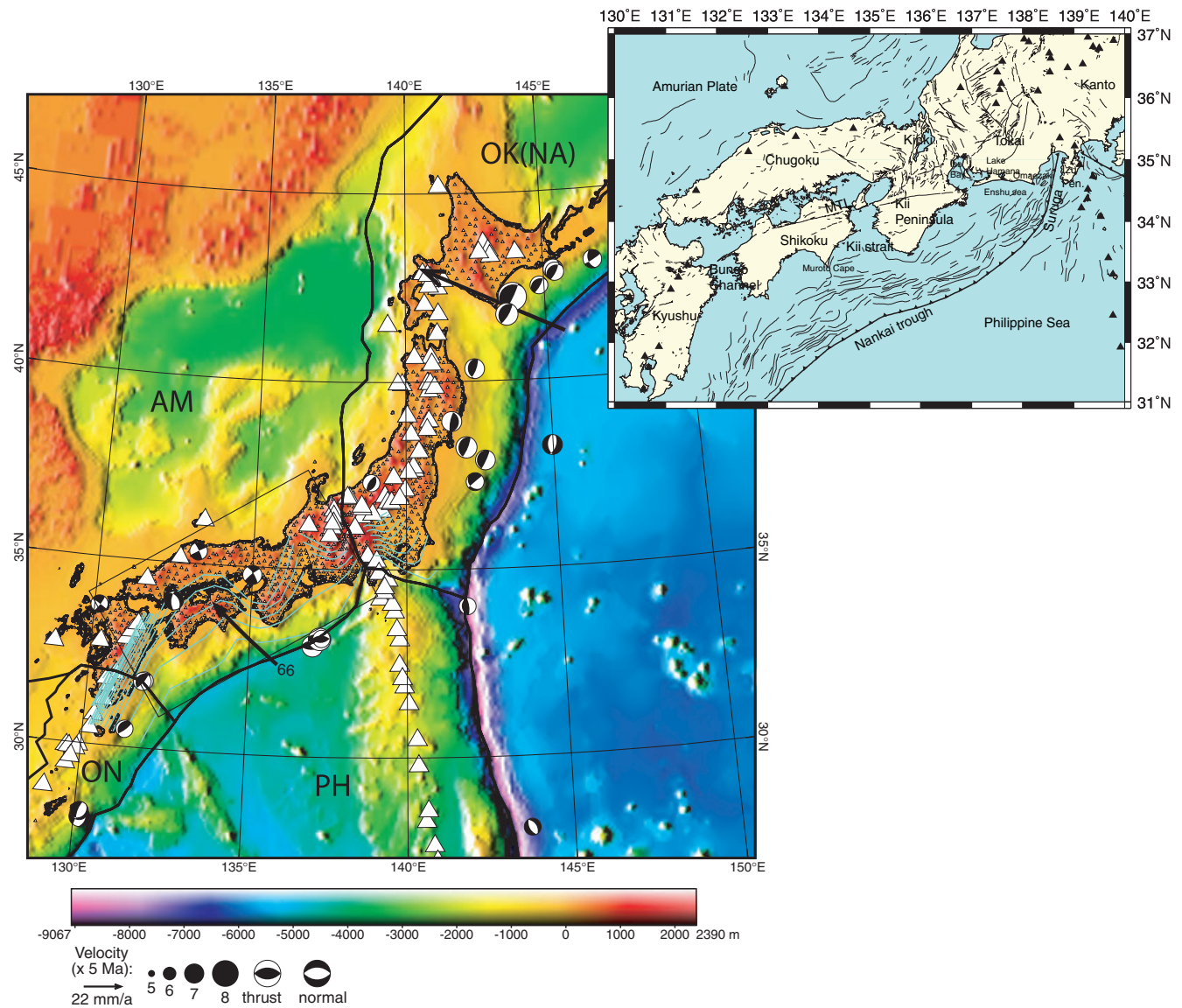


**Figure 1.** Mapview of the tectonic setting of the Japan. Underlying colormap is the topography from ETOPO5. Small open triangles represent the GPS sites of GEONET. White triangles represent volcanoes. The focal mechanisms of large earthquakes with  $M_w > 6$  at the depth range of 0–70 km during 1996–2006 are shown in a lower hemisphere projection. Thin cyan lines are the iso-depth contours of the upper surface of the Philippine Sea plate from Wang *et al.* (2004). Relative motions between Philippine Sea and Amuria Plate, and between Pacific and North America plates are shown by thick vectors. The updated plate boundaries (Bird 2003) are shown by the thick black lines. AM, Amurian Plate; PH, Philippine Sea Plate; ON, Okinawa Plate; PA, Pacific Plate; OK(NA), Okhotsk(North America) Plate. Top inset is the enlarged view of southwest Japan, in which names of tectonic elements discussed in the text are indicated.

common mode error (CME) from raw time-series. We derived both horizontal and vertical velocities using the time-series in the period of 1996–2006 (for most sites, this is equivalent to  $\sim 10$  yr GPS data), and use them to constrain interseismic crustal deformation models of the Nankai subduction zone. The main goal of this study is to re-examine the plate locking distribution on the subduction fault interface in SW Japan using improved GPS data solutions from state-of-the-art analysis and longer data observations, resulting in a better insight into the loading of the subduction interface and its relation to the past and future earthquake generation.

## 2 DATA ANALYSIS

We analysed GPS data from GEONET from 1996 April 1 to 2005 December 30 using the GPS Network Processor (GNP) (Owen *et al.*

2006). The GNP is based on GIPSY/OASIS-II analysis software, developed at the Jet Propulsion Laboratory (JPL), and is designed to provide bias-fixed solutions for large GPS networks through efficient processing on cluster computers. The GNP first generates point-position solutions (Zumberge *et al.* 1997) for all the stations, fixing the satellite clock and orbital parameters to the JPL precise GPS orbits. The point positioned solutions are then used to determine bias-fixed baseline solutions, between a ‘hub’ and ‘spoke’ station. Given the size of the Japan network, many stations were used as hubs. Two iterations of bias-fixing were combined to give a single solution, the first with a maximum baseline length of 250 km, and a second with a maximum baseline length of 50 km. The merged solution was then rotated into ITRF2000.

To separate the secular rate solutions from transient deformation signals and additional atmospheric seasonal and/or site specific

noise sources requires time-series analysis of the daily position solutions. Various regional filtering techniques have been developed to suppress or eliminate common mode noise in GPS position time-series. Wdowinski *et al.* (1997) removed common mode error (CME) from each coordinate component by stacking and computing the daily weighted mean of the position residuals from a set of regional fiducial sites. The mean position residuals are then subtracted from the time-series. This filtering approach reduces the amplitude of white and coloured noise components by a factor of 2–3 (Williams *et al.* 2004). In the present study, we adopted an approach that is based on the Principal Component Analysis (PCA) to remove common mode error and clean up time-series (Aoki & Scholz 2003; Dong *et al.* 2006). In this approach, an empirical model is developed to fit the raw data and obtain the residual time-series. Then PCA is applied on the residual time-series to estimate common mode errors in space and time. Application of this new filtering method in California indicates that it can effectively remove long wavelength CME across the whole network (Dong *et al.* 2006).

We used the time-series analysis module developed by D. Dong at JPL to fit an empirical model to the raw data before estimating the CME. The daily GEONET coordinates were fit by the following empirical model:

$$\begin{aligned}
 x(t) = & a + bt + c \sin(2\pi t) + d \cos(2\pi t) + e \sin(4\pi t) \\
 & + f \cos(4\pi t) \\
 & + \sum_{i=1}^m g_i H(t - t_i) + \sum_{j=1}^n h_j \ln((t - T_j)/\tau_j) H(t - T_j) \\
 & + \sum_{k=0}^3 J_k (t - t_0)^k,
 \end{aligned}$$

where  $x(t)$  is the position component (in metres) of a GPS site at the observation epoch  $t$ , in years, measured from the starting epoch of time-series at the individual site. The reference epoch is 2000.0. On the right hand side, the first two terms are the position bias  $a$  and linear rate  $b$ . The terms  $c$ ,  $d$ ,  $e$  and  $f$  are the amplitudes of sinusoidal annual and semi-annual variations,  $H(t)$  is the step function representing offsets caused by an earthquake, GPS antenna replacement, or unknown source. The units for the position bias ( $a$ ), amplitudes of seasonal variations ( $c$ ,  $d$ ,  $e$  and  $f$ ), and  $g_i$  are in metres. The linear rate ( $b$ ) has unit of metre per year. We model postseismic transient deformation using a logarithmic decay with amplitude  $h_j$  at selected earthquake epochs  $T_j$  and characteristic decay time constant  $\tau_j$ .  $\tau_j$  is set to be 0.01 yr for most postseismic transients. To avoid potential contamination of the CME by unmodelled aseismic transient signals, we identify and model the transient signals using a third-order local polynomial with coefficient  $J_k$ , in which  $J_0$  and  $J_1$  are bias and linear terms. Here  $t_0$  is the starting epoch of the time segment that is fit by the polynomial. Note that the non-steady terms including offsets  $g_i$ , logarithmic fit  $h_j$  and local polynomial  $J_k$  are estimated only when the sites have offsets, post-seismic transients, and other transient signals (e.g. aseismic slip). Since we applied local polynomial fit only to the time period during which transient signals occurred, there is no trade-off between  $J_0$ ,  $J_1$  and  $a$ ,  $b$ . For the Tokai slow slip event (SSE), the transient time period is 1999.8–2004.676. For the Bungo Channel region, the transient time periods are 1996–1998.2 and 2002–2004.3, respectively, when two major SSEs occurred. For sites that are affected by slip transients, the interseismic velocities are estimated using the data that are not affected by transient signals. For example, for the sites in the Tokai region, this would refer to the time period before the onset of the Tokai SSE.

We took an iterative approach to determine the times of offsets and transient deformation in the time-series. In order to determine an initial list of offsets due to seismic events, we developed an earthquake offset predictor program to predict where earthquake related offsets should be set. We used Global CMT Catalogue (downloaded from <http://www.globalcmt.org/CMTsearch.html>) and extracted earthquakes in Japan ([lon. 125–150°E, lat. 25–47°N]) with  $M_w$  6–10 and depth range 0–100 km in the period of 1995 January 1–2006 December 31. For the earthquakes that have available slip distribution from seismic or geodetic inversion, we set source dimensions based on these studies. Otherwise, we adopted a point source approximation by assigning a nominal size of 1 km<sup>2</sup> to the source area. We inferred slip using seismic moment in the CMT and predicted the surface motion using slip estimates and the source dimension. The surface displacement was calculated using an elastic dislocation in a uniform elastic half-space (Okada 1985). For a given earthquake, if the predicted offsets at more than five sites were greater than threshold value set *a priori* (e.g. 5 mm), we added the corresponding offset epoch to the model estimation for all sites that are affected by the earthquake. To ensure the offset determination was not biased by fault plane ambiguity, we tested both nodal planes. We used the GSI database of changes to GPS stations to determine the epochs for estimating offsets caused by equipment changes. We inspected the time-series with the largest coseismic offsets for possible post-seismic signals and estimated post-seismic decay if there were transients. To avoid possible trade-off between the logarithmic fit to the post-seismic signals and the linear trend, we required that, for each station, there must be at least 3 yr data that was not affected by the post-seismic signals during the data period (1996–2006). The position time-series and velocity estimates were checked to ensure the estimates are reasonable. We excluded the stations that have either anomalous time-series, or too short time span (<2 yr), or whose velocities are significantly different from adjacent stations (see Table S4). After the model fit, we inspected the residual time-series for other unmodelled offsets or transient signals. This process was done iteratively until all offsets were identified and the residual time-series were free of identifiable transient signals. As an example, Fig. 2 shows the E, N, U position time-series for station 0437 and model fit. For the entire

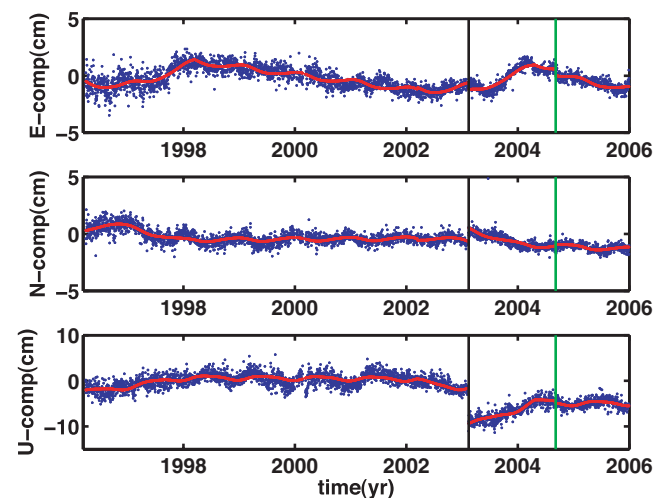


**Figure 2.** Empirical model fit (red curve) to the east component of the raw time-series (blue dots) of station 0437. Both are detrended. Black line represents the offset due to the instrument change. Green line represents earthquake related offset due to  $M_w$  7.4 earthquake on 2004 September 5.

network, the average RMS for the residual time-series is  $\sim 7$  mm, significantly reduced from  $\sim 65$  mm of the initial time-series. It should be noted that, in a companion paper (Liu *et al.* Integration of transient strain events with models of plate coupling and areas of great earthquakes in southwest Japan, manuscript submitted, 2009), we explicitly inverted transient signals from the Tokai and Bungo Channel SSE for transient slip history and examine how slip relates to slow earthquakes and plate coupling.

After generating the residual time-series, we applied a principal component analysis (PCA) to estimate the CME. We choose the first principal component for CME estimates based on an extensive sensitivity study from Dong *et al.* (2006). Details about the PCA estimation can be found in Dong *et al.* (2006). In PCA, we required that each epoch must have at least 30 per cent of stations, and each station must have at least 60 per cent data coverage during the period of 1996–2006. PCA reduces the scattering of the position and, as a result, after removing the CME, the typical repeatability in our analysis for 10 yr is  $\sim 2.4$  mm for the north,  $\sim 3.7$  mm

for the east, and  $\sim 8.3$  mm for the up component. Fig. 3 shows the spatial and temporal response of the first principal component for the GPS east component in the PCA analysis. Fig. 4 shows the comparison of residual time-series before and after PCA. Clearly the removal of the common mode error significantly reduced the scatter in the original time-series. After removing the common mode error, we re-estimated an empirical model using the cleaned time-series. The velocity estimates are then retained for modelling interplate coupling. The resulting RMS of the difference in velocities after the removal of CME is small,  $\sim 0.6$  mm yr $^{-1}$ .

The interseismic velocities were converted from ITRF2000 to Amurian-fixed reference frame using AM-ITRF2000 Euler Pole from Prawirodirdjo & Bock (2004) (Fig. 5, Supplemental appendix Table 1). Formal velocity uncertainties in our data analysis are typically very small:  $\sim 0.09$  mm yr $^{-1}$  for the east,  $\sim 0.07$  mm yr $^{-1}$  for the north, and  $\sim 0.3$  mm yr $^{-1}$  for the vertical component. Previous studies showed that consideration of the coloured noise in the time-series can significantly increase velocity uncertainties (Zhang *et al.*

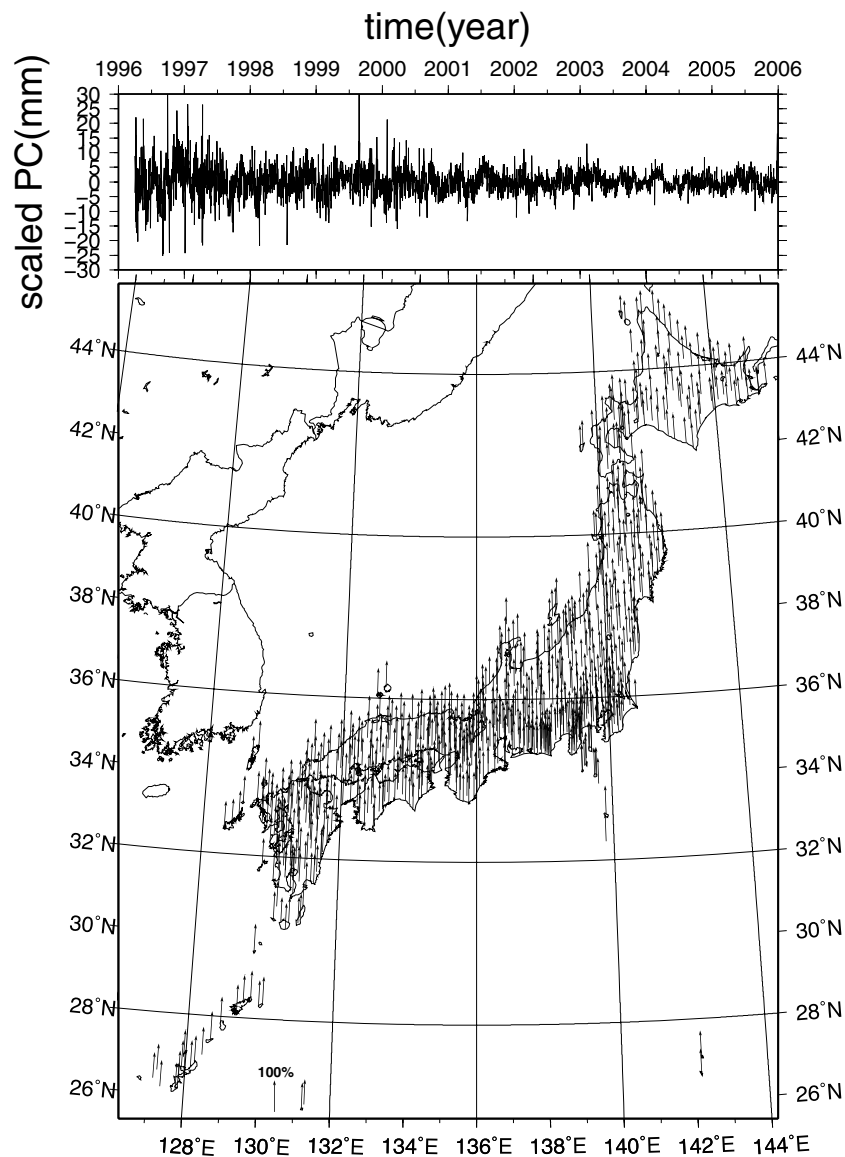


**Figure 3.** East component of the principal component analysis solution. Top panel: first mode of the scaled principal component (PC), and bottom panel: its normalized spatial eigenvectors. The arrows represent the element values of the normalized eigenvectors instead of the velocity directions. The up arrows represent positive spatial responses to the scaled PC while the down arrows represent negative spatial responses to the scaled PC.

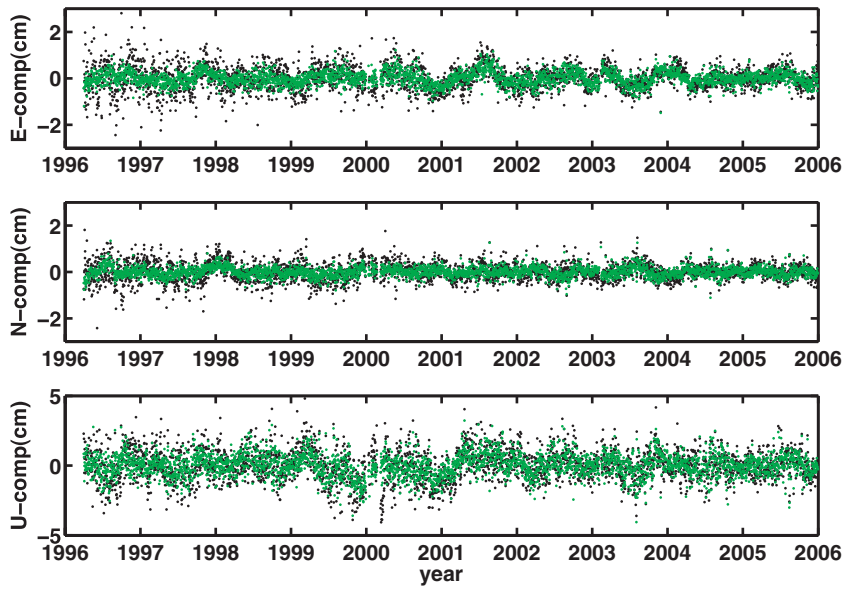


**Figure 4.** Residual time-series before (back dots) and after (green dots) removing the common mode errors. All model terms except seasonal variation are removed from the residual time-series.

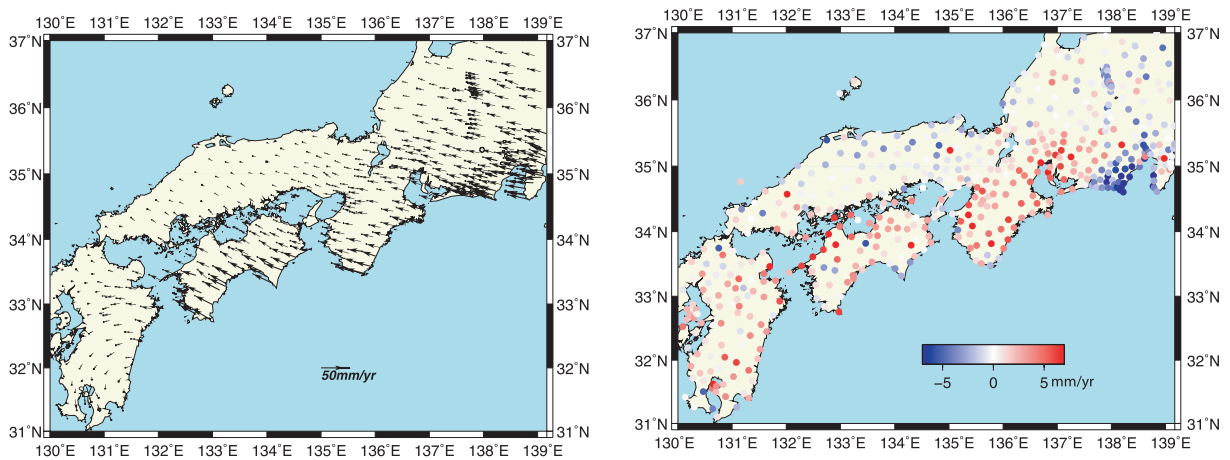


**Figure 5.** Left-hand panel: horizontal velocities in southwest Japan derived from continuous GPS time-series in the period of 1996–2006. The error bars are too small to see ( $\sim 0.1\text{--}3\text{ mm yr}^{-1}$ ). Right-hand panel: vertical velocities in the same time period. Colour scale is saturated at  $-7$  and  $+7\text{ mm yr}^{-1}$  for a better view. S.V. represents Sakurajima volcano. The uncertainties for the vertical velocities are from  $\sim 0.3$  to  $\sim 8\text{ mm yr}^{-1}$ .

**Table 1.** List of experiments with different weights and fault geometry.

Model no.	Fault	Geometry	Weight (horz. vs. vert.)	WRMS ( $\text{mm yr}^{-1}$ )	RMS ( $\text{mm yr}^{-1}$ )	ERMS ( $\text{mm yr}^{-1}$ )	NRMS ( $\text{mm yr}^{-1}$ )	URMS ( $\text{mm yr}^{-1}$ )
SK1	Shikoku-Kii Pen.	Wang-04	2:1	3.54	2.42	1.64	1.63	3.49
SK2	Shikoku-Kii Pen.	Wang-04	1:0.000001	4.00	2.58	1.84	1.80	3.66
SK3	Shikoku-Kii Pen.	Wang-04	1:1	3.95	2.46	1.85	1.79	3.40
SK4	Shikoku-Kii Pen.	Wang-04	1:2	3.94	2.34	1.87	1.79	3.12
SK5	Shikoku-Kii Pen.	Wang-04	1:5	4.03	2.23	1.94	1.81	2.81
T1	Tokai	Wang-04	2:1	5.67	2.55	2.10	1.57	3.55
T2	Tokai	Wang-04	1:0.000001	6.26	2.54	2.35	1.77	3.27
T3	Tokai	Wang-04	1:1	6.25	2.42	2.35	1.82	2.95
T4	Tokai	Wang-04	1:2	6.31	2.34	2.36	1.90	2.69
T5	Tokai	Wang-04	1:5	6.65	2.31	2.48	2.05	2.36
SK-N1	Shikoku-Kii Pen.	Nakajima-07	1:2	3.37	2.13	1.65	1.54	2.91
SK-N2	Tokai	Nakajima-07	1:2	6.39	2.29	2.23	2.07	2.56

1997; Williams 2003; Williams *et al.* 2004; Langbein 2008). We performed maximum likelihood analysis on the residual time-series without CME to infer the colour noise spectral index for sites in SW Japan. We found that they can be mostly characterized by flicker noise. Assuming a white noise plus flicker noise model, we estimated that the mean velocity uncertainties are  $\sim 0.27$ ,  $0.23$  and  $0.85 \text{ mm yr}^{-1}$  for the east, north and up components, respectively. The uncertainty is somewhat smaller than some other studies. For example, Tabei *et al.* (2007) assigned  $0.6$ ,  $0.5$  and  $1.8 \text{ mm yr}^{-1}$  to east, north, and up components in their analysis. The reduced uncertainties are partly due to the longer time interval spanned by our analysis but could also be due to our careful screening and analysis in a uniform manner.

### 3 MODELLING METHOD

We adopt a back-slip model of interplate coupling (Savage 1983). The deformation due to plate subduction is expressed by the sum of steady slip over the entire plate interface, and normal slip (back slip) in the coupling area. The steady slip effect is ignored because it produces no strain, and the dominant deformation is attributed to back slip. Back-slip rate is a representation of slip deficit rate along the subduction interface and we use the terms ‘back-slip’ and ‘slip deficit’ interchangeably throughout the paper. We regard back-slip rate as a proxy for interseismic plate coupling and refer the back-slipping regions as coupled. In this view, the regions with large or small back-slip rates are termed as strongly or weakly coupled. Debate surrounds the terminology within the back-slip model, and a slip-deficit may not always correspond to mechanical coupling (Wang & Dixon 2004; Hetland & Simons 2010). Nevertheless, our modelling provides a kinematic estimate of motion along the subduction interface.

We estimate the slip deficit rate along the subduction interface through an inversion of the interseismic GPS site velocities. The fault geometry is assumed as *a priori* and modelled with a triangular mesh. This ensures the complex 3-D fault geometry can be faithfully represented. In the inversion we seek to minimize the objective function

$$\Phi(m) = \|W(Gm - d)\|_{L_2}^2 + \gamma \|\nabla^2 m\|_{L_2}^2,$$

where  $W^T * W = \Sigma_d^{-1}$ ,  $\Sigma_d$  is the data covariance matrix. The  $G$  is the  $3N \times M$  elastic Green’s function that represents the elastic response at each GPS station for unit slip at each fault patch on the subduction interface. We calculate elastostatic Green’s function using triangular dislocation elements in an elastic half space (Jeyakumar *et al.* 1992). The vector  $d$  is  $3N$ -element data vector that contains the interseismic velocities at  $N$  GPS sites. The model parameter vector  $m$  is obtained by simultaneously minimizing the  $L_2$ -norm of data misfit and of model roughness. Model roughness is defined as the change in fault slip rate per length of fault and typically is in units of  $\text{m/yr/km}$ . The parameter  $\gamma$  controls the relative weight imposed on the model roughness. Minimizing the model roughness leads to a larger misfit but prevents overfitting noisy data and compensates for underdetermined problems and geometry inaccuracy.

We rewrite the inverse problem as

$$\begin{bmatrix} WG \\ \gamma D \end{bmatrix} m = \begin{bmatrix} Wd \\ 0 \end{bmatrix},$$

where  $D = \nabla^2$  represents  $M \times M$  smoothing matrix, quantified by the Laplacian of slip components of adjacent fault patches along the strike and dip of the fault surface. The smoothness constraint  $\gamma D$  is

treated as pseudo-data and applied to both the downdip and along-strike directions. We calculate the discrete form of the Laplacian operator  $\nabla^2$  using a scale-dependent umbrella operator (Desbrun *et al.* 1999) as  $\nabla^2 m_i = \frac{2}{L_i} \sum_{j=1}^3 \frac{m_j - m_i}{h_{ij}}$ , where  $h_{ij}$  represents the distance from the centre of element  $i$  to the centre of its adjacent element  $j$ ,  $m_j$  is the slip vector of element  $j$ , and  $L_i$  is the sum of the element centre distances,  $L_i = \sum_{j=1}^3 h_{ij}$ . The slip at the edge of the fault is constrained to be zero. In addition to smoothing, we also impose positivity constraints on both dip-slip and strike-slip components. This reduces the oscillation in the inverted slip. The positivity constraint is implemented by solving the inverse equation by a nonlinear fast non-negative least squares algorithm (Van Benthem & Keenan 2004). We determine the smoothing factor  $\gamma$  from a trade-off curve that balances both the model roughness and data misfit (Harris & Segall 1987; Du *et al.* 1992).

We constructed the subduction fault geometry using a composite plate interface model of Wang *et al.* (2004). We also tested the alternative fault geometry from Nakajima & Hasegawa (2007). The latter included the results of Baba *et al.* (2002), Hirose *et al.* (2008) and Nakajima *et al.* (2007) Fig. 6 shows the comparison of the iso-depth contours from the two fault models, which are generally similar.

Surface kinematics in southwest Japan is complicated. In addition to the deformation signals induced by plate loading along the subduction interface, other sources exist that contribute to the surface deformation. As shown in Fig. 5, the velocity field in western and southern Kyushu contains clear south or southeastward movement, reflecting possible combined effects from backarc rifting in the Okinawa Trough and central Kyushu, localized Sakurajima volcano deformation (Takayama & Yoshida 2007), and an active left-lateral shear zone in southern Kyushu (Nishimura & Hashimoto 2006; Wallace *et al.* 2009). Site velocities in northeastern Kyushu show continuous NW motion but at reduced amplitude, indicating that the interplate coupling related deformation at least extends to this part of plate boundary (Nishimura & Hashimoto 2006; Takayama & Yoshida 2007; Wallace *et al.* 2009). We select the sites in northeastern Kyushu while ignoring sites in western and southern Kyushu. Correspondingly, we exclude the fault surface beneath the Kyushu area in the inversion. In southwest Japan, the intra-arc collision between NE and SW Japan causes widespread long-term east–west compression in the northeast Inland area (Miyazaki & Heki 2001; Heki & Miyazaki 2001). In central Japan, the Tokai–south Kanto region has been regarded either as the transition from North America to Amurian Plate (Heki & Miyazaki 2001) or to move approximately uniformly as an independent block with regard to the SW and NE Japan arcs (Mazzotti *et al.* 2001; Nishimura *et al.* 2007). The accommodation of PH-AM Plate motion by the Izu microplate and over-riding Tokai block reduces the plate convergence rate beneath the Tokai district by  $\sim 60$  per cent of the original PH-AM convergence rate (Heki & Miyazaki 2001). To avoid attributing non-subduction related deformation to interplate loading, we choose GPS sites that are known to be mainly subject to plate loading processes. Since the Tokai area is affected by long term ‘block-like’ motion, interplate loading, and possibly some effects from the Izu–Bonin arc collision near the Izu Peninsula, we model it separately from the Shikoku and Kii Peninsula. A separate reference site is used in the Tokai model to remove long term block motion. Figs 7 and 8 show the GPS sites and fault surface that we employed in the models of the Shikoku–Kii Peninsula and Tokai.

We neglect the deformation due to strain accumulation on inland faults in SW Japan except for the Median Tectonic Line (MTL). Most of these inland faults have average slip rates of a few  $\text{mm yr}^{-1}$ ,

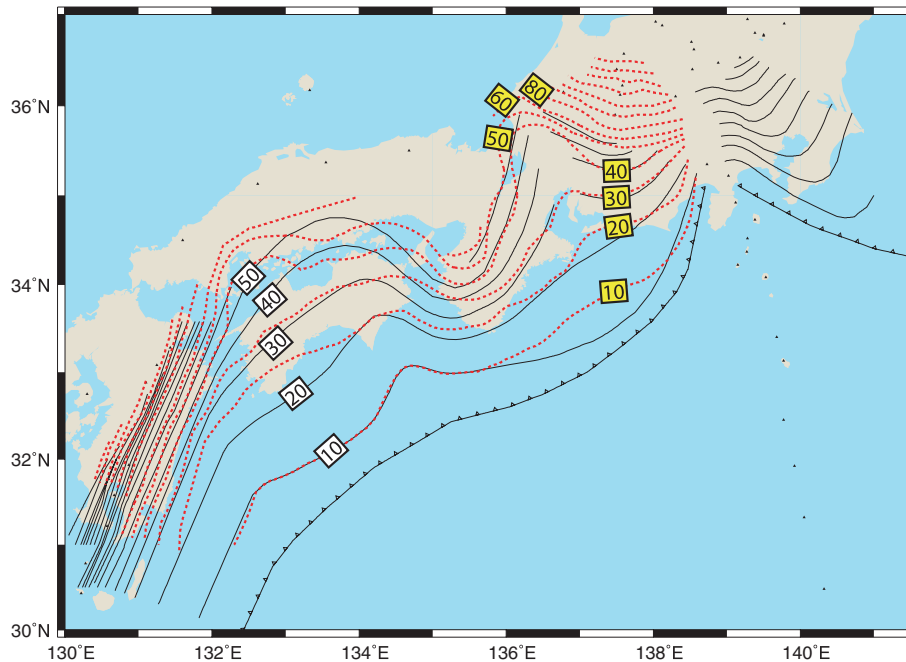


**Figure 6.** Iso-depth contours of the upper plate surface of the Philippine Sea Plate from Wang *et al.* (2004) (thin black line) and Nakajima *et al.* (2007) (red dashed line). The contour interval from Wang *et al.* (2004) is 10 km. The contour interval from Nakajima *et al.* (2007) is 10 km for the depth less than 60 km and 20 km for the deeper depth. We use white and yellow boxes to separate contour levels from these two studies. The contour levels are only labelled up to 50 km for Wang *et al.* (2004) and 80 km for Nakajima *et al.* (2007), respectively.

much smaller than the plate convergence rate. The Median Tectonic Line (MTL) fault is a major right-lateral strike-slip fault running from the Kii peninsula, Shikoku, to eastern Kyushu. We applied a correction for the locking effect on this fault. The MTL has been inferred as an inclined strike-slip fault dipping to the north with a dip angle ranging from  $\sim 35^\circ$  to  $50^\circ$  (Tabei *et al.* 2003, 2007; Kamamura *et al.* 2003; Nishimura & Hashimoto 2006). Previous studies show that it is acting as a boundary fault separating the Shikoku and Kii Peninsula into the inner and the outer arcs (Miyazaki & Heki 2001; Nishimura & Hashimoto 2006; Tabei *et al.* 2007). Nishimura & Hashimoto (2006) estimated that the outer arc (forearc block) moves west or southwestward at a rate of  $\sim 5\text{--}8\text{ mm yr}^{-1}$  relative to the AM plate. Tabei *et al.* (2007) obtained the similar result and found that the outer arc moves at the rate of  $\sim 6.7\text{ mm yr}^{-1}$  parallel to the strike of the MTL. Because we focus on the interplate coupling, we corrected  $\sim 6.5\text{ mm yr}^{-1}$  of the long-term forearc motion (relative to the Amurian plate) from the sites located south of MTL in Shikoku and Kii Peninsula. We also removed the elastic loading effect of the locked MTL from all velocities that are used in the inversion by assuming a dip angle of  $45^\circ$ , locking depth of  $\sim 15\text{ km}$  and back-slip rate that is comparable to the forearc motion. The correction accounts for  $\sim 5$  per cent of the total velocities on average.

Both horizontal and vertical velocities are used in the back-slip inversion. Typically the vertical component has larger uncertainties compared to the horizontal velocities. In this study, the mean vertical uncertainty is approximately four times larger than that of the horizontal velocity component, which gives rise to the horizontal components having four times the weight of the vertical on the model solution. It is well known that the vertical velocity is more sensitive to the plate locking at depths than the horizontal velocity. However, how much weight should be assigned to each velocity component is still not clear. Suwa *et al.* (2006), based on the similarity of the vertical velocity pattern derived from GPS data and

leveling surveys, argued that GPS vertical velocities can be more reliable than their standard errors. As a result, they applied double weight to the vertical data in their NE Japan Plate coupling model. Tabei *et al.* (2007) found that putting equal weight on both horizontal and vertical GPS data in SW Japan improved the resolution of data and reduced the uncertainties associated with estimated parameters. Here, we carried out a series of experiments that tested different relative weighting factors of horizontal to vertical GPS data: (1) 2:1; (2)  $1:10^{-5}$  (only horizontal velocity data were used); (3) 1:1; (4) 1:2 and (5) 1:5. Table 1 lists these experiments and corresponding rms errors. It should be mentioned that these relative weighting factors represent weighting multipliers to the inverse of the formal errors of velocity estimates. Since average velocity uncertainties in horizontal and vertical components are  $\sim 0.25$  and  $\sim 0.85\text{ mm yr}^{-1}$ , the mean actual weights of horizontal to vertical velocities, determined by the formal errors and weighting factors, are  $\sim 6.8:1.0$ ,  $\sim 3.4 \times 10^5:1.0$ ,  $\sim 3.4:1.0$ ,  $\sim 1.7:1.0$  and  $\sim 0.7:1.0$ , respectively. However for simplicity we refer to these relative weighting factors instead of actual weights in the subsequent discussion. Based on the overall RMS misfit, it appears that the cases that have more weight on the vertical GPS data are preferred (e.g. SK4, SK5, T4 and T5). However, increasing vertical weighting five times more causes a larger misfit to the horizontal GPS velocity and a larger weighted RMS (WRMS) but does not result in a significant improvement of the vertical fit. We are also concerned that putting too much weight on the vertical data might force the model to overfit some local non-tectonic noise. Since doubling the relative weight of the vertical component gives a reasonable fit to both horizontal and vertical velocities, and the number of vertical components is half of the horizontal ones, we therefore assigned a double weighting factor to the vertical data in the inversion results discussed in the following section. This corresponds to an actual weight ratio of  $\sim 1.7:1.0$  between the horizontal and vertical GPS data.

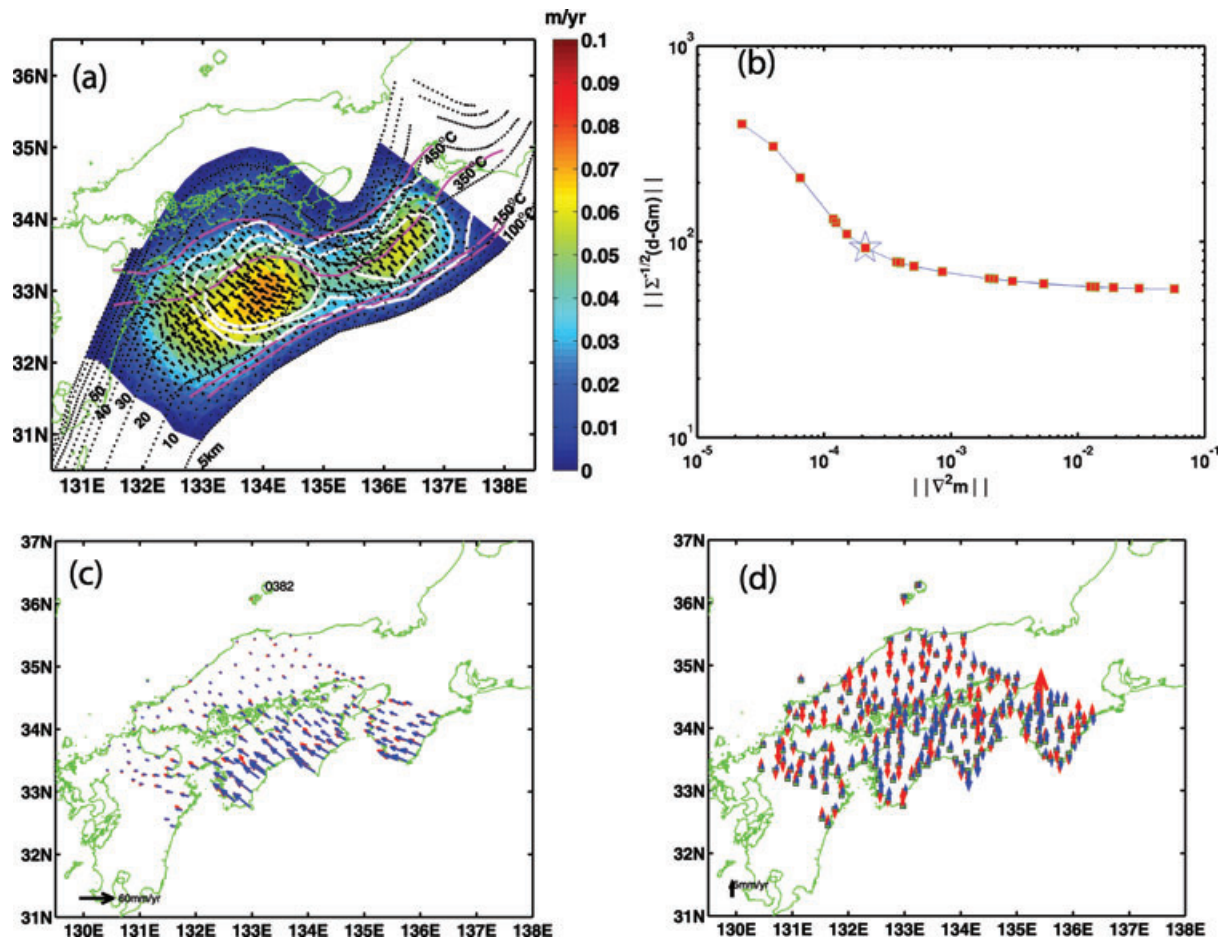


**Figure 7.** (a) Back-slip distribution beneath Shikoku and Kii Peninsula. Dashed lines are the iso-depth contour lines from Wang *et al.* (2004). Magenta lines represent the isothermal lines of 100, 150, 350 and 450 °C from the thermal model of Yoshioka & Murakami (2007). Black vectors are surface projections of back-slip vectors at the centre of fault patches. White lines are the coseismic slip contours from Sagiya & Thatcher (1999). (b) Square root of weighted residual sum of squares (WRSS) versus norm of model roughness. The star indicates the location of the optimal smoothing parameter where the balance between model misfit and smoothness is achieved. (c) Model predicted horizontal velocity using slip deficit in (a) (blue) versus observed horizontal velocity (red). (d) Model predicted vertical velocity (blue) versus observed vertical velocity (red).

## 4 RESULTS

### 4.1 Shikoku and Kii Peninsula

We use three-component velocities to estimate slip deficit beneath the Shikoku and Kii Peninsula. The data are the horizontal and vertical velocities with respect to station 0382 (Fig. 7c), which is the furthest site from the coastline and has an uplift rate that is zero within the uncertainty level. Tests showed that the model fit and inferred back-slip pattern are not sensitive to the choice of inland reference station. We propagate the velocity errors from the reference station to the data covariance. In the inversion, we calculate model predicted velocities with respect to the reference site and compare to the observed velocities (Figs 7c and d). For the regional GPS network, this ensures a consistent frame for both model and data. For this study, we used a total of 185 GPS sites.

We determine the optimal smoothing parameter by constructing a trade-off curve between the model roughness and the model misfit (square root of weighted residual sum of square) (Fig. 7b). The optimal smoothing parameter,  $\lambda$ , corresponds to the roughness of  $\sim 0.2 \text{ mm yr}^{-1} \text{ km}$ . Different choices of  $\lambda$  generate significantly undersmoothed or oversmoothed slip distributions under positivity constraints.

The slip deficit estimates beneath Shikoku and the Kii Peninsula are shown in Fig. 7(a). Also shown are the coseismic slip contours from the 1944 *M*7.9 Tonankai and 1946 *M*8.0 Nankai earthquakes inferred from triangulation data, levelling data, and tidal gauge offsets (Sagiya & Thatcher 1999). The estimated slip deficit pattern shows that the intraplate coupling is strongly depth-dependent. The highly coupled region (with back-slip rate  $> 25 \text{ mm yr}^{-1}$ ) extends from  $\sim 10$  to 30 km in depth with an average back-slip rate of  $\sim 45 \text{ mm yr}^{-1}$ . Plate coupling decreases significantly towards the deeper portions of the plate interface. The decrease towards the shallowest (along the Nankai trough) plate interface ( $< 10 \text{ km}$ ) is not well constrained and mainly attributed to the zero back-slip constraint imposed at the trench axis. The back-slip rate is also spatially non-uniform. For the highly coupled area off Shikoku, the average back-slip rate (or slip deficit rate) is  $\sim 47 \text{ mm yr}^{-1}$ . Off-shore Shikoku there is an area with back-slip rate  $\sim 60\text{--}70 \text{ mm yr}^{-1}$ , implying nearly full locking. In the area off Kii Peninsula the inferred back-slip rate is  $\sim 50\text{--}60 \text{ mm yr}^{-1}$ . El-Fiky *et al.* (1999) used 2-yr GPS data (1996 April 1–1998 March 31) to find the strongly coupled area in Shikoku district at 10–30 km deep with an average back-slip rate of  $43 \pm 5 \text{ mm yr}^{-1}$ . Our results using GPS observations from a much longer time span ( $\sim 10 \text{ yr}$ ), are consistent with these earlier estimates suggesting that within our model resolution,



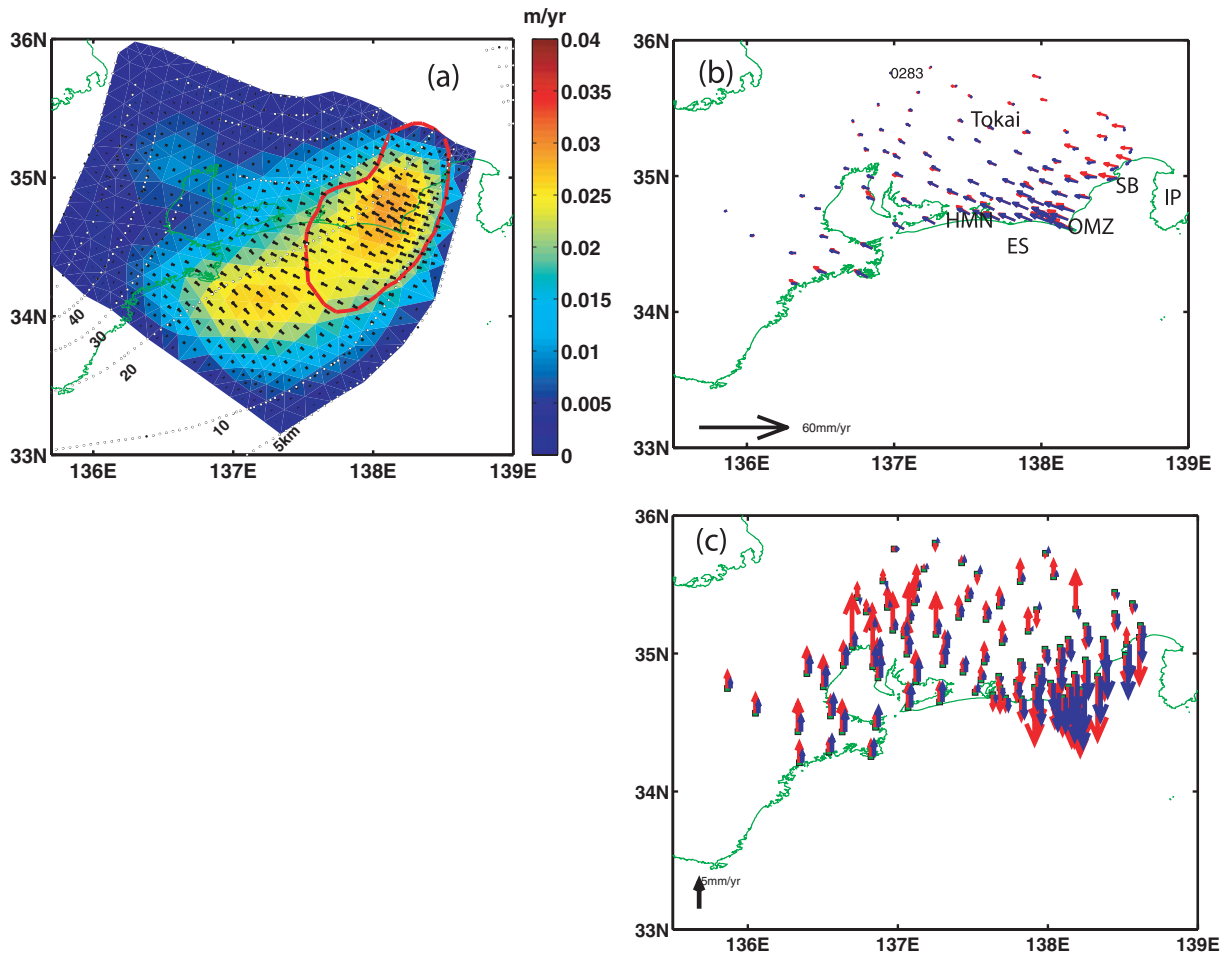


**Figure 8.** (a) Back-slip distribution beneath the Tokai district. Dashed lines represent the iso-depth lines from Wang *et al.* (2004). Red curve shows the anticipated source area of the future Tokai earthquake (Center Disaster Management Council, 2001). (b) Predicted horizontal velocity from the back-slip model (blue) versus observed horizontal velocity (red). (c) Predicted vertical velocity (blue) versus observed vertical velocity (red).

the interseismic coupling on the plate interface does not change much over the time, at least for the period of 1996–2006. Our inverted back-slip vectors in the strongly coupled area are oriented at  $\sim N55 \pm 15^\circ W$ , consistent with relative plate motion predicted from AM-PH Euler vector at the Nankai Trough ( $\sim 63.3$ – $68.7 \text{ mm yr}^{-1}$  towards  $\sim N55W$ ) (Miyazaki & Heki 2001).

We find that the inferred regions of strong coupling agree well with the inferred coseismic rupture zones of the two most recent large megathrust earthquakes in this region (i.e. the 1944 Tonankai and 1946 Tokai earthquakes). The back-slip distribution has two slip maxima areas corresponding to maximum coseismic slip area of the Tonankai and the Nankai earthquake, respectively. A low slip zone beneath the Kii strait separates these maxima.

Figs 7(c) and (d) shows model predicted horizontal and vertical velocities versus observed ones. The velocity residuals between the observations and model prediction are small, with the following RMS values:  $\sim 2.3 \text{ mm yr}^{-1}$  for three components,  $\sim 1.9 \text{ mm yr}^{-1}$  for the east,  $\sim 1.8 \text{ mm yr}^{-1}$  for the north and  $\sim 3.1 \text{ mm yr}^{-1}$  for the vertical component. The reduction in data variance is  $\sim 93.1$  per cent with  $\sim 97$  per cent reduction in the horizontal component and  $\sim 10$  per cent in the vertical. The small variance reduction for the vertical could be attributed to small vertical tectonic signal (e.g.  $< 5 \text{ mm yr}^{-1}$ ) and large noise ( $\sim 2 \text{ mm yr}^{-1}$  for the propagated error) in the region. If we force an unrealistic rougher solution for a

smaller misfit, the variance reduction for the horizontal marginally improves to  $\sim 98$  per cent and vertical variance reduction increases to  $\sim 29$  per cent. However, the improvement in vertical variance reduction is largely dominated by a few isolated sites and overall fit does not change much. This behaviour suggests that vertical component is less consistent and likely affected by other localized non-tectonic deformation (e.g. hydrologic or magmatic sources).

#### 4.2 Tokai district

We performed a similar analysis of plate coupling beneath the Tokai district. GPS stations in the Tokai area are influenced by multiple deformation sources: long term motion of the central Japan block, loading processes due to plate subduction, and long term collision between NE and SW Japan. We chose 90 stations in a relatively narrow zone in Tokai region (Fig. 8) and exclude stations that are mainly affected by intra-arc collision. The velocity estimates are based on the time period prior to the start of the Tokai SSE. We accounted for Tokai transient signals from 1999.8 to 2004.67 through a polynomial fit in the data analysis. Station 0283 is used as the reference point. By referencing relative velocities with respect to a reference site, we removed the effects of block motion. Fig. 8(a) shows the back-slip distribution inferred from

our interseismic velocity estimates. It is clear that maximum slip deficit rate of  $\sim 29 \text{ mm yr}^{-1}$  is detected at the depth of 10–25 km around (138.2E, 34.7N). The highly coupled area with back-slip rate 10–25  $\text{mm yr}^{-1}$  at the depth of 10–25 km extends southward from the Enshu Sea. The back-slip vector direction is relatively uniform with dominant direction oriented to the WNW beneath Omaezaki and Suruga Bay, gradually rotating clockwise to a more NW direction in the western part of the model domain. In the area where the slip deficit is greater than  $10 \text{ mm yr}^{-1}$ , the slip direction is  $\text{N}60.5^\circ \pm 11.5^\circ \text{W}$ . This is in general agreement with predicted plate convergence direction ( $\text{N}59^\circ \pm 6^\circ \text{W}$ ) from the Euler pole of Izu microplate with respect to the Amurian Plate (Heki & Miyazaki 2001). Our inferred slip deficit rate agrees with a previous estimate of the plate convergence rate ( $\sim 20\text{--}30 \text{ mm yr}^{-1}$ ) in Suruga bay (Heki & Miyazaki 2001).

Our model is consistent with the earlier results of Ohta *et al.* (2004) who used 3-D velocities of 69 sites distributed in the Tokai region during the period 1997–2000 to estimate the interplate coupling. They found a maximum slip deficit rate ( $<30 \text{ mm yr}^{-1}$ ) at a depth of 15–25 km around the Enshu Sea. They also found a northward extension of the high slip deficit area. In contrast, Sagiya (1999) obtained a maximum slip deficit rate  $\sim 30\text{--}40 \text{ mm yr}^{-1}$  under the Enshu Sea, larger than what we obtained. We are concerned that such estimates may be too large compared to the plate convergence rate inferred for this region (Heki & Miyazaki 2001).

The back-slip model provides a reasonable fit to most stations (Figs 8b,c). The RMS misfit is  $\sim 2.3 \text{ mm yr}^{-1}$  for three components,  $\sim 2.4 \text{ mm yr}^{-1}$  for the east,  $\sim 1.9 \text{ mm yr}^{-1}$  for the north, and  $\sim 2.7 \text{ mm yr}^{-1}$  for the vertical. The reduction in data variance is  $\sim 81$  per cent. A few stations northeast of Omaezaki have larger misfits. These stations locate above the region where PH slab geometry is not well known (Fig. 6). To test whether these larger misfits may be caused by the limited extent of our assumed fault surface, we extrapolated our model surface but found that the fit only improved slightly, while the inferred distribution of back slip remains almost unchanged. Given that the sites with larger misfits are spatially close to the collision front of Izu-Bonin arc and have negligible contribution to the slip, we are not overly concerned about their misfit. If we exclude these stations, we have a total variance reduction of about 89 per cent, which can be broken down to a 94 per cent for the horizontal components and 72 per cent for the vertical components. The RMS misfits for both the Shikoku and Kii Peninsula and the Tokai district are several times the formal errors in the data. This could be due to the limitation of the simple back-slip model or some unmodelled non-tectonic factors, or a combination of both.

### 4.3 Model resolution and uncertainty

We are obviously concerned about the reliability of the inferred slip pattern since the geodetic network is located onshore while the seismogenic interface extends offshore. It is known that onshore GPS networks are typically less able to resolve offshore slip (Nishimura & Hashimoto 2006). We test our model resolution by performing a checkerboard test, which has been used to illustrate the resolution power of GPS networks (e.g. Hsu *et al.* 2006). We compute surface velocities from a synthetic checkerboard-like slip distribution on the plate interface. Both downdip and strike slip components are assigned to alternate slip patches such that the slip rate is  $\sim 7 \text{ cm yr}^{-1}$  beneath Shikoku and the Kii Peninsula area and  $\sim 4 \text{ cm yr}^{-1}$  beneath the Tokai district. We calculate predicted displacements from the synthetic slip distribution and supplement them with random noise

that is assumed to be Gaussian with zero mean and the same standard deviation as the real data ( $\sim 0.3 \text{ mm yr}^{-1}$  for the horizontal and  $\sim 1 \text{ mm yr}^{-1}$  for the vertical). The same inversion method is applied to the synthetic GPS data as was applied to the real data, and results for this checkerboard test are shown in Fig. 9. For Shikoku and the Kii Peninsula, the GPS network and inversion method used in this study can successfully resolve slip beneath the land area and updip extension to a depth of  $\sim 10$  km but cannot resolve slip at shallower depths. For the Tokai area, most slip beneath the land area and near the coastline can be resolved. The slip further offshore southwest of the Enshu Sea cannot be reliably estimated. We performed a similar test on the downdip resolution (not shown here). We assign the synthetic slip to the region at the depth range of 10–30 km on the plate interface. Then the synthetic observations with added random noise were inverted. The results show that the downdip limit of the coupling can be recovered satisfactorily.

Model parameter uncertainties cannot be easily estimated by error propagation from the data covariance because of the non-negativity constraints. Instead, we estimate uncertainties of model parameters using a Monte Carlo simulation. A synthetic velocity field was generated from the estimated slip deficit with random noise added (assumed to be Gaussian with zero mean and the same variance as the real data). The same smoothing factor is adopted because the data variance and fault geometry remains the same. The synthetic data was then inverted, and we repeated this process for  $\sim 1000$  times, each time with different random noise added to the synthetic velocity field. This test gives a sense of how sensitive the estimated slip values are to the error distribution at the GPS stations. To determine the extent of variation, the RMS of the difference in slip on each fault patch between the inverted and the input was computed. The results show that the maximum RMS difference in the slip estimate is small:  $<10 \text{ mm yr}^{-1}$  beneath the Shikoku and Kii Peninsula and  $<5 \text{ mm yr}^{-1}$  beneath the Tokai district.

### 4.4 Geometry effects

We tested an alternative interplate geometry based on Nakijima *et al.* (2007) to evaluate the sensitivity of our results to the fault geometry (SK-N1, SK-N2 in Table 1). As shown in Fig. 6, the main difference between Nakijima's and Wang's plate geometry lies in the shallow portion at depths of  $\sim 10\text{--}30$  km. The inverted back-slip pattern using Nakajima's fault geometry is shown in Fig. 10. It is clear that both geometries produced a very similar slip distribution, as compared to the slip in Figs 7(a) and 8(a). The maximum back-slip rate in Nakijima's model is slightly less than that in Wang's model. However, overall, the effect of changing fault geometry is minor.

## 5 DISCUSSION

Vertical GPS velocities have long been thought to be more sensitive to the interplate coupling effect on subduction zone faults (Lundgren *et al.* 1999; Aoki & Scholz 2003). However, they are not often used because of much lower signal-to-noise ratio. It is less clear how well the vertical rates can help to resolve the back-slip distribution. In NE Japan, Suwa *et al.* (2006) found that using three components of GPS site velocities improved model fit and resolution, although they needed to assume that all the observed vertical signals result from the plate loading process. In SW Japan, both horizontal and vertical crustal motion seem to be consistent with the back-slip model prediction (Aoki & Scholz 2003; Heki

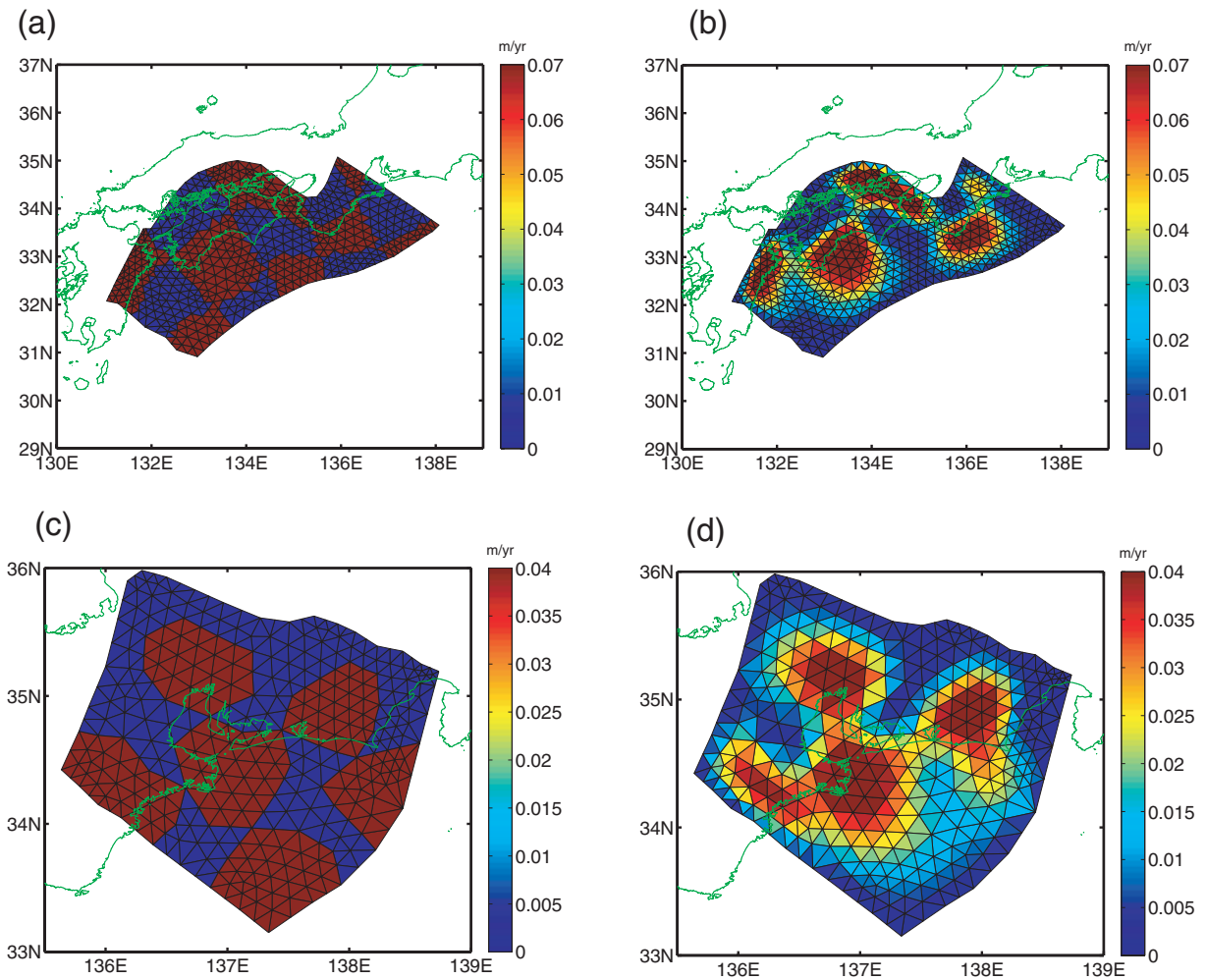


**Figure 9.** (a) Synthetic checkerboard-like slip model with slip rate  $7 \text{ cm yr}^{-1}$  on the plate interface under Shikoku and Kii Peninsula. (b) Recovered slip distribution using the same inversion method and station distribution as in real data. All positive slip patches are recovered successfully except the ones at depths shallower than  $\sim 10 \text{ km}$ . (c) Synthetic slip model with slip rate  $4 \text{ cm yr}^{-1}$  on the plate interface beneath the Tokai district. (d) Recovered slip distribution. Slip on the fault patches southwest of Enshu Sea is not well resolved.

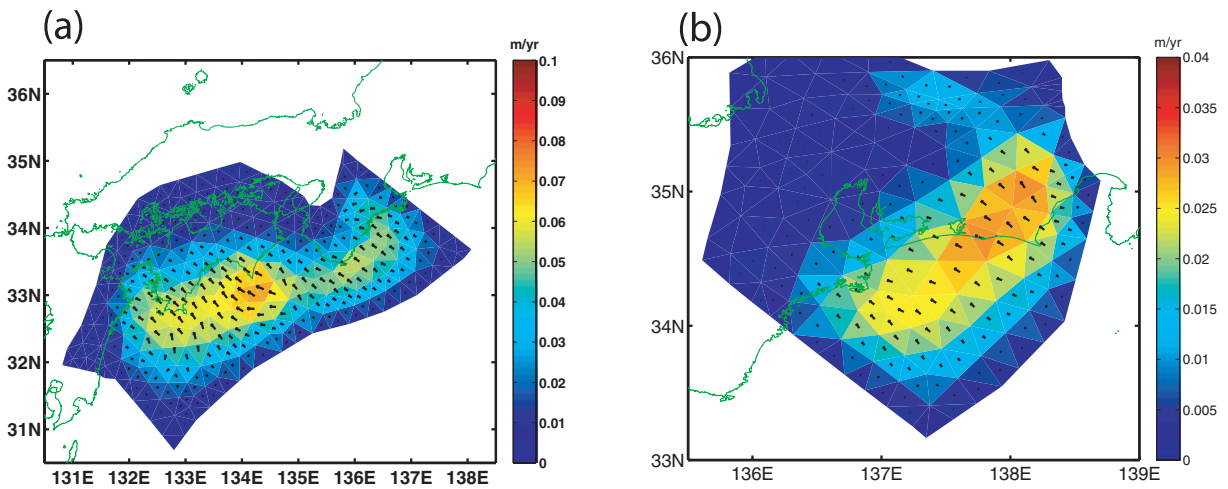


**Figure 10.** (a) Inverted back-slip beneath Shikoku and Kii Peninsula using alternative fault geometry of Nakajima *et al.* (2007). (b) Inverted back-slip on the new plate geometry beneath Tokai district.

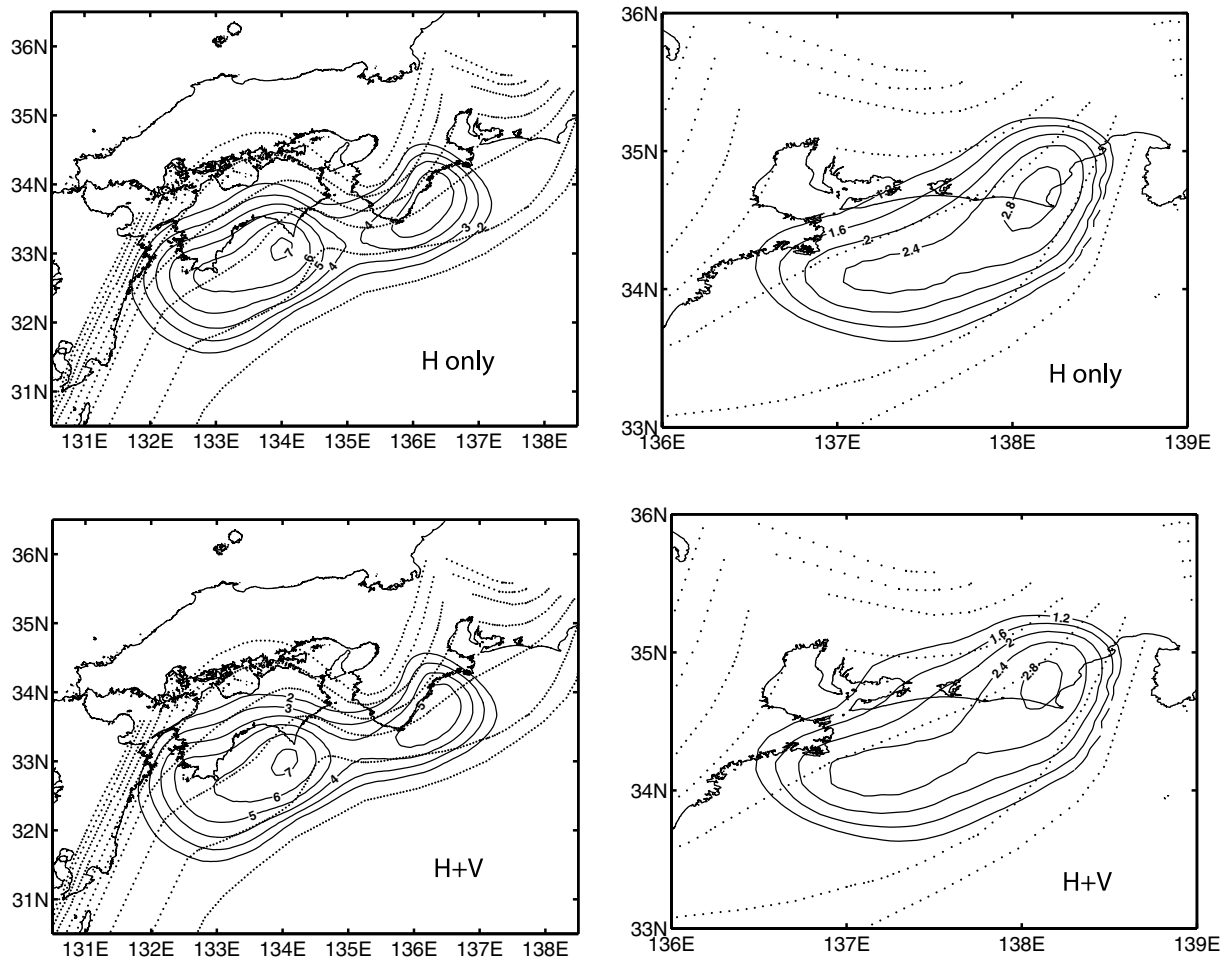


**Figure 11.** Back-slip distribution using only horizontal velocity data beneath the Shikoku and Kii Peninsula (a) and the Tokai district (b) versus back slip using both horizontal and vertical velocity data (c, d).

2007). Tabei *et al.* (2007) found slightly stronger coupling at the transitional depth of 25–35 km when the vertical velocities were appropriately weighted. In this study, we varied weighting for both horizontal and vertical velocity data. By setting different weighting on the vertical data, we were able to estimate the contribution from the vertical data to back-slip distribution. Fig. 11 shows the comparison of slip deficits derived from only horizontal velocity (SK2, T2) versus from both horizontal and vertical data (SK4, T4). The overall pattern is quite similar. However close examination reveals some differences. For example, the downdip transition zone from the strongly coupled area to the weakly coupled zone is sharper and shallower beneath Kii Peninsula when the vertical velocity data are used. Southwest off Shikoku the high slip deficit region with slip rate of  $60 \text{ mm yr}^{-1}$  or more is shallower and spatially more limited when both horizontal and vertical data are used. Also, in the Tokai district, the use of all three components of the velocity produce a spatially more limited region of high slip deficit near Omaezaki and Suruga Bay and a slightly wider downdip extent of the transition zone. It is well known that the vertical velocities are most sensitive to the variations in coupling strength and spatial distribution near the downdip transition zone while the horizontal velocities are not so strongly affected (Tabei *et al.* 2007). Therefore, the differences we observed directly reflect the contribution from vertical velocities. The relatively small variance reduction that occurs when we enhance the weighting of the vertical components may be ex-

plained by the sensitivity of the vertical component to other processes other than subduction zone coupling, such as anthropogenic hydrologic signals, which also affect the horizontal to a lesser degree (Argus *et al.* 2005). Our results suggest that the vertical velocities are generally consistent with back-slip predictions but provide more resolving power on the details of the transition zone.

The estimated slip deficit beneath Shikoku and Kii Peninsula (Fig. 7a) indicates strong coupling at a depth of 10–30 km. Less coupling is found at the shallow depth of  $\sim 5$ –10 km. This is different from some other studies (Mazzotti *et al.* 2000; Miyazaki & Heki 2001; Nishimura and Hashimoto 2006; Tabei *et al.* 2007), in which nearly full locking was suggested at those shallow depth range. The difference mainly arises from *a priori* information assumed about the back slip on the fault segments near the Nankai trough. We employ a constraint of zero back slip (i.e. fully decoupled) at the trench axis, whereas Tabei *et al.* (2007) and others assumed full coupling at shallow depth. Nevertheless, the resolution test indicates that on-land GPS data provide little resolution on the fault slip shallower than 10 km.

Most importantly, the upper and lower limit of a transition zone in Tabei *et al.* (2007) was fixed to be 25 and 35 km, and slip deficit within the transition zone was assumed to decrease linearly to nearly zero below 35 km. In this study, we estimate plate coupling without imposing any constraint on the depth extent of a transition zone. The results show that the lower limit of the transition zone extends

deeper than 35 km. Our inferred coupling strength has both depth dependency and lateral variation in the depth range of the transition zone.

Variations in temperature on megathrusts are frequently hypothesized to be one of the primary controls on the coupling strength (e.g. Hyndman & Wang 1993; Hyndman *et al.* 1995; Oleskevich *et al.* 1999). Hyndman *et al.* (1995) suggested that the temperature is the dominant control on the updip and downdip limit of seismogenic portion of subduction thrust faults. For southwest Japan, they estimated that the updip limit of coseismic dislocation and of interseismic elastic strain build-up was  $\sim 30$  km landward from the trench (corresponding to  $\sim 150$  °C) while the downdip extent of the fully locked zone and the transition zone is limited by the temperature of 350 and 450 °C, respectively. Yoshioka & Murakami (2007) obtained a similar conclusion by using an improved 3-D thermal model that included an accurate slab shape and more heat flow data. In Fig. 7(a) the downdip limit of the strongly coupled region and transition zone correspond very well to the temperature of 450 °C derived from independent thermal estimates. The maximum coseismic slip and highly coupled area locates well within the thermal regime that has temperature less than 350 °C. The strong correspondence between our geodetically inferred regions of strong coupling and thermal modelling results is consistent with the hypothesis that the spatial limit for seismic behaviour is thermally controlled. Nevertheless, despite good success of thermal control on coupling strength, the low coupling beneath the Kii Strait remains a mystery. It appears to be shallower than the temperature of 450 °C. Possibly other factors such as steep slab geometry change or the subducting of islandarc type crust (Seno & Yamasaki 2003) beneath the Kii Strait, as discussed more below, could also affect the plate coupling and its relation to the local thermal structure.

Recently, slow earthquakes such as non-volcanic tremor and low frequency earthquakes (LFE) were discovered at the downdip portion of seismogenic zone in southwest Japan (Obara 2002). There seems to be a close correlation between the lateral variation of estimated plate coupling, LFEs [Akio Katsumata, personal communication], and coseismic slip distributions (Fig. 12). Beneath the Shikoku and Kii Peninsula, the LFEs coincide well with  $\sim 450$  °C isotherm, which may be related to the phase transformation of hydrous materials in the subducting oceanic crust and fluid release (Yoshioka & Murakami 2007). Offshore of the Shikoku and Kii Peninsula we see the large coupling and coseismic slip maximum, accompanied by the belt-like LFE distribution inland. Beneath the Kii Strait there is lower coupling and smaller coseismic slip as well as a gap in the LFE distribution. The lateral variation may be closely related to the change of plate geometry configuration. As shown in Fig. 6, the Philippine Sea slab changes to a higher dip angle near the Kii Strait, as compared to more planar-like, shallower dip below Shikoku and the Kii Peninsula. Similarly, no LFEs occur beneath southern Kyushu where the slab dip angle becomes much higher. In the Tokai district, a LFE gap was observed below Ise Bay where the slab geometry changes significantly. Noticeably, the slab geometry at shallow depth in the same region remains relatively smooth so the slip deficit pattern is not disrupted. The heterogeneity in slab geometry could affect the thermal structure on the plate interface, and thus cause variation of the seismogenic zone (Yoshioka & Murakami 2007). Recent seismological observations suggest that fluids from metamorphic dehydration of the subducting plate may play a role in the occurrence of LFE/tremor and slip transients in the southwest Japan (e.g. Peacock 2009; Matsubara *et al.* 2009). The fluid release may be related to the thermal structure and metamorphic environment (Peacock 2009). It is possible that the geometry

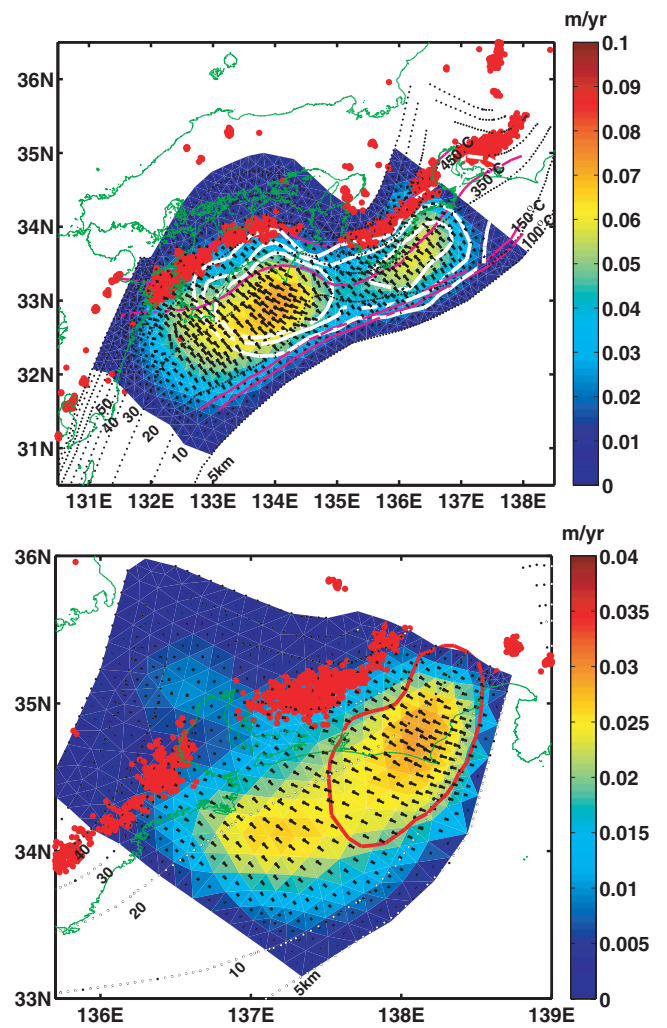


**Figure 12.** Top panel: back-slip distribution beneath the Shikoku and Kii Peninsula overlaid with the epicentres of low frequency earthquakes (LFEs; red dots). Other symbols are the same as in Fig. 7(a). Bottom panel: back-slip distribution beneath the Tokai district overlaid with LFEs.

could affect thermal structure and metamorphic environment thus influencing slab dehydration and the extent of fluid release. Recent seismic imaging of the  $V_p/V_s$  ratio and correlation with tremor activity beneath SW Japan seems to support this view (Matsubara *et al.* 2009). The slab geometry could also affect the lateral variation of frictional properties, which would affect earthquake nucleation as suggested by recent numerical experiments (Hori *et al.* 2004). In addition, slab geometry irregularity may act as natural barrier to prevent rupture from propagating through the entire plate segment (Sagiya & Thatcher 1999). Seno & Yamasaki (2003) proposed an alternative hypothesis that attributes the lack of LFE beneath Southern Kyushu, east Shikoku and N. Izu-Kanto region to the subduction of less hydrated island-arc type crust. Although it is not clear which hypothesis is more viable, the effects from slab geometry should not be completely excluded.

Strong coupling ( $> 50$  per cent) at depths 10–30 km with maximum (nearly 100 per cent coupling) located around  $\sim 20$  km beneath Shikoku and the Kii Peninsula is generally consistent with previous studies despite different data analysis techniques, inversion methods and plate geometries adopted by these studies (e.g. El-Fiky *et al.*

1999; Ozawa *et al.* 1999; Heki and Miyazaki 2001; Miyazaki & Heki 2001; Ito & Hashimoto 2004; Jin *et al.* 2007; Tabei *et al.* 2007; Wallace *et al.* 2009). Our back slip estimates beneath the Tokai district shows strong coupling (>40 per cent) at a depth of 10–25 km, also comparable to previous studies (Ohta *et al.* 2004; Miyazaki *et al.* 2006). This general agreement indicates that the interplate coupling does not display significant variation over the GPS observation period (1996–2006). One notable feature in our model result is the large slip deficit ( $\sim 4\text{--}5\text{ cm yr}^{-1}$ ) below western Shikoku, which extends further downdip. Wallace *et al.* (2009) obtained the similar findings beneath western Shikoku. Part of the area overlaps with the source region of long term transient slip that occurred in 1996–1998 and 2002–2004 beneath the Bungo Channel (Ozawa *et al.* 2007), indicating that some of the interseismic slip deficit is released by episodic transient slip. The estimate of total slip deficit budget in the area requires detailed imaging of spatiotemporal slip distribution of these transient events that are investigated in details in a companion study (Liu *et al.* 2010).

In the models for the Shikoku-Kii Peninsula and Tokai region, we use a reference station and consider relative velocities in our modelling. This helps to put the data frame and the reference frame defined by the dislocation model into a consistent frame. An implication of using velocities relative to a single reference station is that we cannot accurately estimate block rotations. However, being able to fit both horizontal and vertical velocity components with a single model and good agreement of our inferred slip deficit distribution with previous studies suggests that such rotational effects due to the use of a reference site for our study areas are minor. If significant block rotations of the plate boundary zone with respect to the reference site were present, the increased weighting of the vertical component might be expected to change significantly the modelled horizontal vectors. Since this is not the case it lends support to there being no significant rotations relative to the reference site.

## 6 CONCLUSIONS

We applied a network processing strategy to reprocess GPS data from GEONET from 1996 to 2006. We performed careful time-series analysis on the resulting GPS solutions. By employing principal component analysis, we removed spatially correlated common mode error and these improved GPS time-series were used to estimate interseismic velocities. We estimated plate coupling along the interface through back-slip inversions of the velocity field. We corrected the velocity field for the forearc movement and locking effects from the Median Tectonic Line, and tested various weighting on the horizontal and vertical velocity data. We find that the combined use of both horizontal and vertical data improves the resolution of the transition zone. The estimates of back-slip show a strong coupling at the depth of 10–30 km beneath the Shikoku and Kii Peninsula. The slip deficit is spatially non-uniform exhibiting both downdip and along strike variation with slip maxima corresponding well with coseismic rupture zones of past large earthquakes. The plate interface in the Tokai and Suruga Bay is strongly locked at the depth of 5–25 km with maximum slip deficit rate of  $\sim 25\text{--}30\text{ mm yr}^{-1}$ . The downdip and updip limit of the highly coupled region and transition zone coincide well with the bounding limits of the seismogenic zone inferred from thermal models, supporting the traditional view of temperature control on the coupling strength in southwest Japan. Low frequency earthquakes appear to occur at the downdip edge of the highly coupled region, consistent with previous findings (e.g. Shelly *et al.* 2006; Schwartz & Rokosky 2007). Their correlation

with spatial variations in slab dip seems to suggest that temperature and possibly fluid variation associated with slab dehydration may be affected by the plate geometry heterogeneity.

## ACKNOWLEDGMENTS

We thank K. Wang and Junichi Nakajima for sending us their composite plate geometry model for the Philippine Sea slab. We thank Akio Katsumata at Meteorological Research Institute, Japan for providing us low frequency earthquake catalogue. We also thank GSI for providing us the raw data of GEONET. Reviews by J. Freymueller, L. Wallace, and editor J. Beavan improved this manuscript. The research described in this paper was carried out at the Jet Propulsion Laboratory, California Institute of Technology, under a contract with the National Aeronautics and Space Administration and funded through the internal Research and Technology Development Program. This research was supported in part by the Gordon and Betty Moore Foundation. This is Caltech Tectonic Observatory Contribution 109.

## REFERENCES

- Ando, M., 1975. Source mechanism and tectonic significance of historical earthquakes along the Nankai Trough, Japan, *Tectonophysics*, **27**, 119–140.
- Aoki, Y. & Scholz, C. H., 2003. Vertical deformation of the Japanese islands, *J. geophys. Res.*, **108**, 1996–1999, B5, 2257, doi:10.1029/2002JB002129.
- Argus, D., Heflin, M., Peltzer, G., Crampe, F. & Webb, F. H., 2005. Interseismic strain accumulation and anthropogenic motion in metropolitan Los Angeles, *J. geophys. Res.*, **110**, B04401, doi:10.1029/2003JB002934.
- Baba, T., Tanioka, Y., Cummins, P. R. & Uhira, K., 2002. The slip distribution of the 1946 Nankai earthquake estimated from tsunami inversion using a new plate model, *Phys. Earth planet. Inter.*, **132**, 59–73.
- Bird, P., 2003. An updated digital model of plate boundaries, *Geochem. Geophys. Geosyst.*, **4**(3), 1027, doi:10.1029/2001GC000252.
- Desbrun, M., Meyer, M., Schröder, P. & Barr, A. H., 1999. Implicit fairing of irregular meshes using diffusion and curvature flow, in *Proceedings of the 26th Annual Conference on Computer Graphics and Interactive Techniques*, pp. 317–324, ACM Press/Addison-Wesley Publishing Co., New York, NY, doi:10.1145/311535.311576.
- Du, Y., Aydin, A. & Segall, P., 1992. Comparison of various inversion techniques as applied to the determination of a geophysical deformation model for the 1983 Borah Peak earthquake, *Bull. seism. Soc. Am.*, **82**(4), 1840–1866.
- Dong, D., Fang, P., Bock, Y., Webb, F., Prawirodirdjo, L., Kedar, S. & Jamason, P., 2006. Spatiotemporal filtering using principal component analysis and Karhunen-Loeve expansion approaches for regional GPS network analysis, *J. geophys. Res.*, **111**, B03405, doi:10.1029/2005JB003806.
- El-Fiky, G. S., Kato, T. & Oware, E. N., 1999. Crustal deformation and interplate coupling in the Shikoku district, Japan, as seen from continuous GPS observations, *Tectonophysics*, **314**, 387–399.
- Hetland, E. & Simons, M., 2010. Postseismic and interseismic fault creep II: transient creep and interseismic stress shadows on magathrusts, *Geophys. J. Int.*, **181**, 99–112, doi:10.1111/j.1365-246X.2010.04482.x.
- Harris, R. A. & Segall, P., 1987. Detection of a locked zone at depth on the Parkfield, California, segment of the San Andreas fault, *J. geophys. Res.*, **92**, 7945–7962.
- Heki, K., 2007. Secular, transient and seasonal crustal movements in Japan from a dense GPS array: implications for plate dynamics in convergent boundaries, in *The Seismogenic Zone of Subduction Thrust Faults*, pp. 512–539, ed. Dixon, T. and Moore, C., Columbia University Press, New York.
- Heki, K. & Miyazaki, S., 2001. Plate convergence and long-term crustal deformation in central Japan, *Geophys. Res. Lett.*, **28**(12), 2313–2316.

- Henry, P., Mazzotti, S. & Pichon, X. L., 2001. Transient and permanent deformation of central Japan estimated by GPS 1. Interseismic loading and subduction kinematics, *Earth planet. Sci. Lett.*, **184**, 443–453.
- Hori, T., Kato, N., Hirahara, K., Baba, T. & Kaneda, Y., 2004. A numerical simulation of earthquake cycles along the Nankai Trough in southwest Japan: lateral variation in frictional property due to the slab geometry controls the nucleation position, *Earth planet. Sci. Lett.*, **228**, 215–226.
- Hirose, F., Nakajima, J. & Hasegawa, A., 2008. Three-dimensional seismic velocity structure and configuration of the Philippine Sea slab in southwestern Japan estimated by double-difference tomography, *J. geophys. Res.*, **113**, B09315, doi:10.1029/2007JB005274.
- Hsu, Y. J. *et al.*, 2006. Frictional afterslip following the 2005 Nias-Simeulue earthquake, Sumatra, *Science*, **312**, 5782, 1921–1926, doi:10.1126/science.1126960.
- Hyndman & Wang, K., 1993. Thermal constraints on the zone of major thrust earthquake failure: the Cascadia subduction Zone, *J. geophys. Res.*, **98**(B2), 2039–2060.
- Hyndman, R. D., Wang, K. & Yamano, M., 1995. Thermal constraints on the seismogenic portion of the southwestern Japan subduction thrust, *J. geophys. Res.*, **100**(B8), 15 373–15 392.
- Ito, T., Yoshioka, S. & Miyazaki, S., 1999. Interplate coupling in southwest Japan deduced from inversion analysis of GPS data, *Phys. Earth planet. Inter.*, **115**, 17–34.
- Ito, T. & Hashimoto, M., 2004. Spatiotemporal distribution of interplate coupling in southwest Japan from inversion of geodetic data, *J. geophys. Res.*, **109**, B02315, doi:10.1029/2002JB002358.
- Jeyakumaran, M., Rudnicki, J. W. & Keer, L. M., 1992. Modeling slip zones with triangular dislocation elements, *Bull. seism. Soc. Am.*, **83**(5), 2153–2169.
- Jin, H. L., Kato, T. & Hori, M., 2007. Estimation of slip distribution using an inverse method based on spectral decomposition of Green's function utilizing Global Positioning System (GPS) data, *J. geophys. Res.*, **112**, B07414, doi:10.1029/2004JB003378.
- Kawamura, T., Onishi, M., Kurashimo, E., Ikawa, T. & Ito, T., 2003. Deep seismic reflection experiment using a dense receiver and sparse shot technique for imaging the deep structure of the Median Tectonic Line (MTL) in east Shikoku, Japan, *Earth Planets Space*, **55**, 549–557.
- Langbein, J., 2008. Noise in GPS displacement measurements from southern California and southern Nevada, *J. geophys. Res.*, **113**, B05405, doi:10.1029/2007JB005247.
- Liu, Z., Owen, S., Dong, D., Lundgren, P., Webb, F., Hetland, E. & Simons, M., 2010. Integration of transient strain events with models of plate coupling and areas of great earthquakes in southwest Japan, *Geophys. J. Int.*, **181**, 1292–1312, doi:10.1111/j.1365-246X.2010.04599.x (this issue).
- Lundgren, P., Protti, M., Donnellan, A., Heflin, M., Hernandez, E. & Jefferson, D., 1999. Seismic cycle and plate margin deformation in Costa Rica: GPS observations 1994–1997, *J. geophys. Res.*, **104**, 28 915–28 926.
- Matsubara M., Obara, K. & Kasahara, K., 2008. High-Vp/Vs zone accompanying non-volcanic tremors and slow-slip events beneath southwestern Japan, *Tectonophysics*, **472**, 6–17, doi:10.1016/j.tecto.2008.06.013.
- Mazzotti, S., Le Pichon, X., Henry, P. & Miyazaki, S.-I., 2000. Full interseismic locking of the Nankai and Japan-west Kurile subduction zones: An analysis of uniform elastic strain accumulation in Japan constrained by permanent GPS, *J. Geophys. Res.*, **105**(B6), 13 159–13 177.
- Mazzotti, S., Henry, P. & Pichon, X. L., 2001. Transient and permanent deformation of central Japan estimated by GPS, 2. Strain partitioning and arc-arc collision, *Earth planet. Sci. Lett.*, **184**, 455–469.
- Miyazaki, S. & Heki, K., 2001. Crustal velocity field of southwest Japan: subduction and arc-arc collision, *J. geophys. Res.*, **106**(B3), 4305–4326.
- Miyazaki, S., Segall, P., McGuire, J. J., Kato, T. & Hatanaka, Y., 2006. Spatial and temporal evolution of stress and slip rate during the 2000 Tokai slow earthquake, *J. geophys. Res.*, **111**, B03409, doi:10.1029/2004JB003426.
- Nakajima, J. & Hasegawa, Y., 2007. Subduction of the Philippine Sea plate beneath southwestern Japan: slab geometry and its relationship to arc magmatism, *J. geophys. Res.*, **112**, B08306, doi:10.1029/2006JB004770.
- Nishimura, S. & Hashimoto, M., 2006. A model with rigid rotations and slip deficits for the GPS-derived velocity field in Southwest Japan, *Tectonophysics*, **421**, 187–207.
- Nishimura, T., Sagiya, T. & Stein, R. S., 2007. Crustal block kinematics and seismic potential of the northernmost Philippine Sea plate and Izu microplate, central Japan, inferred from GPS and leveling data, *J. geophys. Res.*, **112**, B05414, doi:10.1029/2005JB004102.
- Obara, K., 2002. Nonvolcanic deep tremor associated with subduction in southwest Japan, *Science*, **296**, 1679–1681.
- Ohta, Y., Kimata, F. & Sagiya, T., 2004. Reexamination of the interplate coupling in the Tokai region, central Japan, based on the GPS data in 1997–2002, *Geophys. Res. Lett.*, **31**, L24604, doi:10.1029/2004GL021404.
- Okada, Y., 1985. Surface deformation due to shear and tensile faults in a half-space, *Bull. seism. Soc. Am.*, **75**, 1135–1154.
- Oleskevich, D. A., Hyndman, R. D. & Wang, K., 1999. The updip and downdip limits to great subduction earthquakes: thermal and structural models of Cascadia, south Alaska, SW Japan, and Chile, *J. geophys. Res.*, **104**(B7), 14 965–14 991.
- Owen, S. E., Dong, D., Webb, F. H., Newport, B. J. & Simons, M., 2006. Deformation of Japan as measured by improved analysis of GEONET data, *EOS, Trans. Am. geophys. Un.*, **87**(52), Fall Meet. Suppl., Abstract G42A-07.
- Ozawa, T., Tabei, T. & Miyazaki, S., 1999. Interplate coupling along the Nankai Trough off southwest Japan derived from GPS measurements, *Geophys. Res. Lett.*, **26**(7), 927–930.
- Ozawa, S., Suito, H., Imakiire, T. & Murakami, M., 2007. Spatiotemporal evolution of aseismic interplate slip between 1996 and 1998 and between 2002 and 2004, in Bungo Channel, Southwest Japan, *J. geophys. Res.*, **112**, B05409, doi:10.1029/2006JB004643.
- Peacock, S., 2009. Thermal and metamorphic environment of subduction zone episodic tremor and slip, *J. geophys. Res.*, **114**, B00A07, doi:10.1029/2008JB005978.
- Prawirodirdjo, L. & Bock, Y., 2004. Instantaneous global plate motion model from 12 years of continuous GPS observations, *J. geophys. Res.*, **109**, B08405, doi:10.1029/2003JB002944.
- Sagiya, T., 1999. Interplate coupling in the Tokai District, Central Japan, deduced from continuous GPS data, *Geophys. Res. Lett.*, **26**(15), 2315–2318.
- Sagiya, T. & Thatcher, W., 1999. Coseismic slip resolution along a plate boundary megathrust: the Nankai Trough, southwest Japan, *J. geophys. Res.*, **104**(B1), 1111–1129.
- Savage, J. C., 1983. A dislocation model of strain accumulation and release at a subduction zone, *J. geophys. Res.*, **88**, 4983–4996.
- Schwartz, S. Y. & J. M. Rokoosky, 2007. Slow slip events and seismic tremor at circum-pacific subduction zones, *Rev. Geophys.*, **45**, RG3004, doi:10.1029/2006RG000208.
- Seno, T. & Yamasaki, T., 2003. Low-frequency tremors, intraslab and interplate earthquakes in southwest Japan—from a viewpoint of slab dehydration, *Geophys. Res. Lett.*, **30**(22), 2171, doi:10.1029/2003GL018349.
- Shelly, D. R., Beroza, G. C., Ide, S. & Nakamura, S., 2006. Low frequency earthquakes in Shikoku, Japan and their relationship to episodic tremor and slip, *Nature*, **442**, 188–191.
- Suwa, Y., Miura, S., Hasegawa, A., Sato, T. & Tachibana, K., 2006. Interplate coupling beneath NE Japan inferred from three-dimensional displacement field, *J. geophys. Res.*, **111**, B04402, doi:10.1029/2004JB003203.
- Tabei, T., Hashimoto, M., Miyazaki, S. & Ohta, Y., 2003. Present-day deformation across the southwest Japan arc: oblique subduction of the Philippine Sea plate and lateral slip of the Nankai forarc, *Earth Planets Space*, **55**, 643–647.
- Tabei, T., Adachi, M., Miyazaki, S., Watanabe, T. & Kato, S., 2007. Interseismic deformation of the Nankai subduction zone, southwest Japan, inferred from three-dimensional crustal velocity fields, *Earth Planets Space*, **59**, 1073–1082.
- Takayama, H. & Yoshida, A., 2007. Crustal deformation in Kyushu derived from GEONET data, *J. geophys. Res.*, **112**, B06413, doi:10.1029/2006JB004690.
- Van Benthem, M. H. & Keenan, M. R., 2004. Fast algorithm for the solution of large-scale non-negativity-constrained least squares problems, *J. Chemometrics*, **18**, 441–450, doi:10.1002/cem.889.
- Wallace, L. M., Ellis, S., Miyao, K., Miura, S., Beavan, J. & Goto, J., 2009. Enigmatic, highly active left-lateral shear zone in southwest

- Japan explained by aseismic ridge collision, *Geology*, **37**, 143–146, doi:10.1130/G25221A.1.
- Wdowinski, S., Bock, Y., Zhang, J., Fang, P. & Genrich, J., 1997. Southern California Permanent GPS Geodetic Array: spatial filtering of daily positions for estimating coseismic and postseismic displacements induced by the 1992 Landers earthquake, *J. geophys. Res.*, **102**(B8), 18 057–18 070.
- Wang, K. L., Wada, I., Ishikawa, Y., 2004. Stresses in the subducting slab beneath southwest Japan and relation with plate geometry, tectonic forces, slab dehydration, and damaging earthquakes, *J. geophys. Res.*, **109**, B08304, doi:10.1029/2003JB002888.
- Wang, K. & Dixon, T., 2004. “Coupling” semantics and science in earthquake research, *EOS, Trans. Am. Geophys. Un.*, **85**, 181–182.
- Williams, S. D. P., 2003. The effect of coloured noise on the uncertainties of rates estimated from geodetic time series, *J. Geodyn.*, **76**, 483–494.
- Williams, S. D. P., Bock, Y., Fang, P., Jamason, P., Nikolaidis, R. M., Prawirodirdjo, L., Miller, M. & Johnson, D. J., 2004. Error analysis of continuous GPS position time series, *J. geophys. Res.*, **109**, B03412, doi:10.1029/2003JB002741.
- Yoshioka, S. & Murakami, K., 2007. Temperature distribution of the upper surface of the subducted Philippine Sea plate along the Nankai Trough, southwest Japan, from a three-dimensional subduction model: relation to large interplate and low-frequency earthquakes, *Geophys. J. Int.*, **171**, 302–315, doi:10.1111/j.1365-246X.2007.03510.x.
- Zhang, J., Bock, Y., Johnson, H., Fang, P., Williams, S., Genrich, J., Wdowinski, S. & Behr, J., 1997. Southern California Permanent GPS Geodetic Array: error analysis of daily position estimates and site velocities, *J. geophys. Res.*, **102**(B8), 18 035–18 055.
- Zumberge, J. F., Heflin, M. B., Jefferson, D., Watkins, M. & Webb, F. H., 1997. Precise point positioning for the efficient and robust analysis of GPS data from large networks, *J. geophys. Res.*, **102**, 5005–5017.

## SUPPORTING INFORMATION

Additional Supporting Information may be found in the online version of this article:

**Table S1.** Velocities (unit: mm yr<sup>-1</sup>) in ITRF2000 from GPS sites in southwest Japan.

**Table S2.** Offset estimates and uncertainties (unit: mm).

**Table S3.** List of sites with transient time period.

**Table S4.** Sites excluded from velocity analysis.

**Table S5.** Estimates of seasonal variation (amplitude and phase).

**Table S6.** Principal components from the PCA analysis.

**Table S7.** Eigenvectors from the PCA analysis.

Please note: Wiley-Blackwell are not responsible for the content or functionality of any supporting materials supplied by the authors. Any queries (other than missing material) should be directed to the corresponding author for the article.